Energy Efficiency (2020) 13:1245–1262
https://doi.org/10.1007/s12053-020-09881-5

ORIGINAL ARTICLE

Research on the thermal performance of rack-level composite baffle diversion system for data centre

Xuetao Zhou · Xiaolei Yuan · Xinjie Xu · Jinxiang Liu · Risto Kosonen · Chao Liu

Received: 18 November 2019 / Accepted: 26 June 2020 / Published online: 17 July 2020

Abstract Airflow management plays an important role in ensuring secured and energy-efficient operation of data centres (DCs). Higher power density in DC is a risk resulting in serious deterioration of airflow distribution accompanied by the increasing cooling energy demand. In this study, the airflow optimization effects of rack baffles and server lower-side terminal baffles on the thermal environment are first validated by experiments. Then, the optimization mechanisms of the two baffle systems are analysed by numerical simulations. The results show that the optimization mechanisms of these two systems are different and the combination can contribute to better airflow distribution than separate baffles. The analysis is validated by altogether 12 cases in 3 scenarios where different combinations of the two systems were included. The results validated the combination of 8 cm × 45° server lower-side terminal baffles and 20 cm × 75° rack baffles can further improve the airflow distribution and relieve heat accumulation in the DC. The impacts of combined baffle system on the thermal environment in DC are analysed by experiments and simulations. The combined system superposes the airflow optimization functions of the two systems. The maximum temperature drop of the hotspot is 0.7 °C, which is 0.4 °C lower than that when only optimal rack baffles or server lower-side terminal baffles are installed.

Keywords Data centres · Airflow management · Rack baffles · Server terminal baffles · Airflow distribution

X. Zhou · X. Xu · J. Liu · R. Kosonen
Department of HVAC, College of Urban Construction, Nanjing Tech University, P.O. Box 76, Nanjing 210009, China

X. Yuan (✉)
School of Mechanical Engineering, Tongji University, 4800 Cao'an Road, Shanghai 201804, China
e-mail: damon01_yuan@tongji.edu.cn

X. Yuan · R. Kosonen
Department of Mechanical Engineering, School of Engineering, Aalto University, P.O. Box 14400, FI-00076 Aalto, Finland

C. Liu
Information Center of Jiangpu Campus, Nanjing Tech University, Nanjing 211800, China

Introduction

The development of information technology (IT) has brought great convenience to mankind. A new level of transformation in data centres (DCs) is driven by the emergence and development of new technologies such as Internet of Things, artificial intelligence and 5th generation. DCs are usually physical spaces that house computer systems and associated devices (such as communication and storage systems) for processing, storing, transferring, exchanging, and managing data. They also contain data communication connections, environmental control equipment, monitoring equipment, and various security devices (Joshi and Joshi 2012; Ashrae 2011). During the past two decades, the development and application of emerging technologies have brought about the explosive growth of data. In response to related demands, the number of DCs has been rapidly

growing (Dayarathna et al. 2016; Zhang et al. 2010). However, an increasingly serious energy crisis comes with this rapid growth because large DCs consume as much electricity as a small town industrial business (Mittal 2014). In addition, the heat dissipation per unit area significantly increases in the operation and maintenance processes of DCs (Dewan and Srivastava 2015). The global energy consumption of DCs is estimated at 416 TWh per year (Avgerinou et al. 2017), which is significantly higher than the total energy consumption of the UK (approximately 300 TWh). Koomey pointed out that the energy consumption of DCs doubles every 4 years, and DCs accounted for approximately 1.3% of the total global electricity consumption in 2010 (Ham et al. 2015a). Consequently, DCs have become more energy consumption than conventional office buildings. In addition, DC is the fastest growing carbon footprint sector in the entire IT industry, accounting for 2% of global carbon dioxide emissions (Avgerinou et al. 2017).

Because the thermal environment of the electronic equipment in DCs is critical to the operation safety of data processing, the appropriate temperature and humidity must be maintained. Currently, the air-conditioning system in DCs needs to operate continually 365 days a year (Kurkjian and Glass 2007). According to a survey conducted by www.researchandmarkets.com (Yuan et al. 2019), the global DC cooling market is expected to exceed $8 billion by 2023. The overall energy consumption of a DC is mainly composed of two parts as follows: IT equipment (e.g. servers, storage, and network) and infrastructure (e.g. cooling system). Analyses of the power consumption of DCs showed that a considerable portion of this usage (approximately 40%) is typically for powering the cooling system (Habibi Khalaj and Halgamuge 2017; Ham et al. 2015b). The major power consumers are the chillers, which supply chilled water to the cooling coils to maintain the indoor environment conditions by removing the heat dissipated by the servers (Joshi and Joshi 2012; Schmidt et al. 2005 ; Siriwardana et al. 2013; Siriwardana 2012; Siriwardana et al. 2012). Hence, it is necessary to reduce the power consumption of DC cooling systems through thermal management techniques.

However, also optimal cooling energy distribution inside the DCs is as important as powering the cooling system. The low cooling efficiency of DCs is mainly due to the uneven airflow distribution (Qian et al. 2013, 2015; Zhang et al. 2018; Sakanova et al. 2019), the resistance of piping systems (Boucher et al. 2006), and high energy consumption of the cold source (Cho and Kim 2016; Ma et al. 2016). At present, experts have proposed several methods for improving cooling efficiency and reducing energy consumption in DCs. Among them, free cooling and airflow management are the most widely used (Oró et al. 2015). The free cooling technology is an ideal method. When the outdoor temperature or sea water temperature is lower than the indoor temperature, the data center is cooled by natural cold source (Pawlish and Aparna 2010). The power usage effectiveness (the ratio of the total power consumed by the data centre to that consumed by the IT equipment) value approaches 1 and the green level of the DC is higher. Existing methods include the direct introduction of outdoor air or water into the DC and utilizing outdoor cold energy by heat exchangers, rotary heat wheel, or two-phase thermosyphon (Zhang et al. 2014; Le Masson et al. 2012; Daraghmeh and Wang 2017; Wang et al. 2019a, b; Phan et al. 2019; Zou et al. 2019; Chauhan and Kandlikar 2019).

Typically, the cooling energy required is transferred to computer room air-conditioner (CRAC) with air. The airflow management strategies are dedicated to changing the DC configuration and CRAC air supply status to improve the cooling efficiency and thermal environment. There are two ventilation methods in conventional DCs as follows: one is up-supply and down-return, while the other is up-return and down-supply. Wang et al. (Wang et al. 2015) found that the height of a raised floor causes significant impacts on the airflow distribution. They proposed a drawer-type rack, which increases the effective hot aisle space and reduces the cold aisle space. With this design, hot air recirculation and cold air bypass will be significantly reduced. Ni et al. (Ni et al. 2017) pointed out that the airflow distribution through the tiles has an important influence on the cooling of computer equipment, and the airflow distribution is more uniform when the air outlet is at an angle of 60° from the tiles. In addition, Nada et al. (Nada and Elfeky 2016) conducted experimental studies on airflow and thermal management of DCs for different arrangements of cold aisle containments, which indicated that the thermal performance of fully enclosed cold aisles is optimal. Subsequently, Zhang et al. (Zhang et al. 2017) investigated the airflow optimization for a small-scale DC with a cold aisle closure. They concluded that the cold aisle closure can optimize the thermal environment in addition to eliminating the bypass airflow.

Many researchers have shown that the application of baffles can significantly improve the airflow effect; therefore, such techniques have been widely investigated. Schmidt et al. (Schmidt et al. 2007) claimed that the installation of baffles can reduce the mixing of hot and cold airflow and improve the airflow distribution in racks. The fan power consumption in IT equipment can be greatly reduced by the efficient use of baffles, and the likelihood of hotspots in DCs can be reduced simultaneously.

The rack baffles can effectively improve the heat distribution in the DC, and the wider the rack baffles, the better the heat distribution in the DC. In recent years, some new methods of applying flexible baffles (FBs) have been studied. The installation of FBs can improve the airflow configuration in DCs without changing their overall structure. FBs are suitable for both new and renovated DCs. In addition, this method requires only a partial modification of the rack level, and there is no need to adjust the air supply parameters of air conditioning. Furthermore, no additional energy consumption is required.

The optimal configuration of FBs has been proposed by Yuan et al. (Yuan et al. 2018, 2019). The application of 20-cm rack baffles tilted to 75° resulted in the most uniform temperature distribution in the rack air outlet, and the hotspot temperature of the rack was reduced by 1.5 °C. In addition, they also applied baffles in the lower terminal of servers and concluded that 8 cm × 45° server terminal baffles can make the rack air outlet temperature distribution more uniform, with the temperature of the rack hotspot reduced by 2.5 °C. The server terminal baffles can also effectively improve the heat distribution in the rack air outlet. Separately, the effect of rack and server terminal baffles on the airflow pattern and heat distribution have been studied by Yuan et al. (Yuan et al. 2018, 2019). However, the integration simultaneously of both rack and server baffles has not received much attention. As the density of racks in DCs continues to increase, the optimization effect of a single baffle system on airflow organization is no longer sufficient. Therefore, the novelty of this study is to combine rack baffle and server baffle system and analyse the optimization effect of the combined system. This study is an extension of the separate previous studies on rack baffles (Yuan et al. 2018, 2019) and server baffles (Yuan et al. 2019). Existing studies on FBs in DCs are verified and analysed. Besides, the optimization mechanisms of these two baffle systems are analysed and validated.

This paper is organized as follows. The first section describes the current state of DC cooling and energy conservation. Then, a combined baffle system using rack baffles and server terminal baffles is proposed. In the second section, a new experimental DC and a new numerical model are introduced. The third section presents the experimental validation on the optimal combination of the rack and server baffle systems in DCs. The velocity fields are analysed to investigate the optimization mechanism of the combined baffle system and numerical simulations are used to verify the results. The optimized combined system is established and analysed, and the simulation results are verified by experiments in the fourth part. Finally, the conclusions are drawn in the last section.

Methodology

Description of the test DC

The DC used for the experiment and simulation is located in a university in Nanjing, China, which operates all year round. This DC has three data rooms, namely, the core DC, super DC, and managed DC. The experiment was carried out in the managed DC. This DC has one air-cooled CRAC (Model TDAR1822, Schneider Electric), and the air supply ducts are installed under the plenum. Figure 1 shows a photo of the DC, which employs a cold aisle containment with the air supplied from an underfloor plenum. The layout of the racks in the test DC is shown in Fig. 2. Perforated tiles are located in the cold aisle to supply cold air to the servers. The hot air discharged by the server fans is extracted by the CRAC unit to re-cool and supplied to the DC plenum. This cooling strategy prevents recirculation of the hot air discharged from the servers and mixing with the supplied cold air from the perforated tiles. The server location in each rack is different, and the number and specification of the servers configured in the racks vary; therefore, the power requirement of each rack differs. Table 1 lists the geometry and technical parameters of the DC for this experiment.

Experimental setup

Experimental validations were conducted in 2019 in an operating DC during June to verify separately the effectiveness of rack baffles and server terminal baffles in

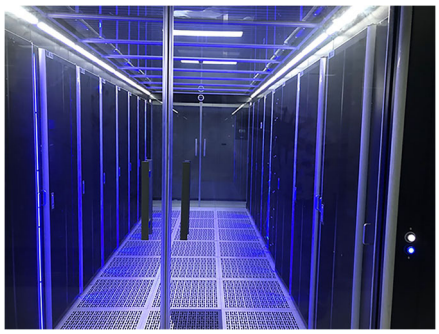

Fig. 1 Analysed data centre

optimizing the thermal environment of the DC. In the experiment, we chose a different rack from previous studies. The experimental procedure is as follows: (1) select a rack with higher power density which is suitable for installing both the rack baffles and server terminal baffles, (2) measure the thermal distribution and possible rack hotspots of the rack airflow outlet, and (3) apply the rack baffles and server terminal baffles to the rack to optimize the airflow distribution and reduce the temperature of the rack outlet. Yuan et al. (Schmidt et al. 2007) defined the rack hotspot as the point where the highest exhaust temperature of the rack is located.

This experiment selected rack B4 for the validation of the combined baffles. The total power of the rack B4 is 16.98 kW. Its rack power density is high, which satisfies the requirement of the experiment, and the layout of the server is relatively uniform. The layout and rated power of the servers in the rack B4 are shown in Fig. 3. All servers have a size of 0.09 m (H) × 0.46 m (W) × 0.8 (L) m. In this experiment, nine temperature test points were set in the rack B4, where each measuring point was located at the central line of the rack rear

Table 1 Specifications of DC components

DC components	Value/notes
Dimensions of DC	9.2 m (L) × 8 m (W) × 4 m (H)
Supply plenum height	0.45 m
Dimensions of CRAC	1.8 m × 0.8 m × 2.25 m
Dimensions of each rack	2.2 m × 0.6 m × 1.2 m
	Rack A and Rack B
The dimension of perforated tiles	0.6 m × 0.6 m
	Total of 24 in three rows
Area of each air vent of CRAC	0.45 m^2
The porosity of perforated tiles	45%
The porosity of front/rear door of each rack	65%
Dimensions of servers in the rack B4	0.09 m × 0.46 m × 0.8 m
	0.09 m × 0.46 m × 0.7 m
	0.045 m × 0.46 m × 0.8 m
	0.18 m × 0.46 m × 0.8 m
Rated power of servers in actual DC	300 W × 2 495 W × 2
	600 W × 2 750 W × 2
	900 W × 2 2000 W × 2

door to ensure that the temperature sensor measures a more uniform air temperature at the air outlet of the rack. The arrangement of the measuring points is presented in Fig. 4.

K-type thermocouples were used as temperature sensors to measure the supply air temperature (SAT) of the rack B4, and Agilent 34,970 Data Acquisition was used for recording data. The temperature sensors were arranged in one-to-one correspondence with the measuring points. The first temperature sensor was located

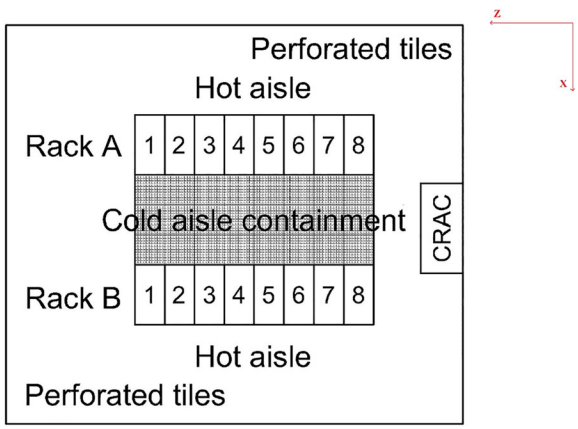

Fig. 2 Schematic of experimental DC

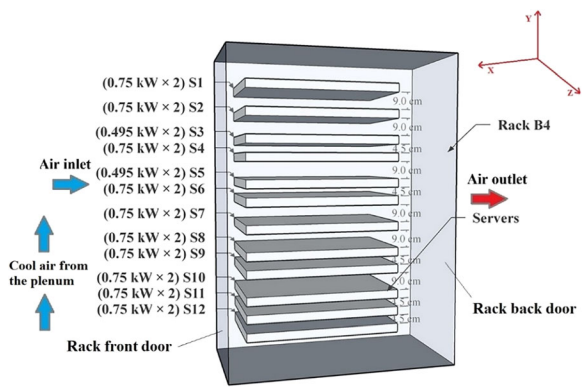

Fig. 3 The layout of servers in the rack B4 (three-dimensional view)

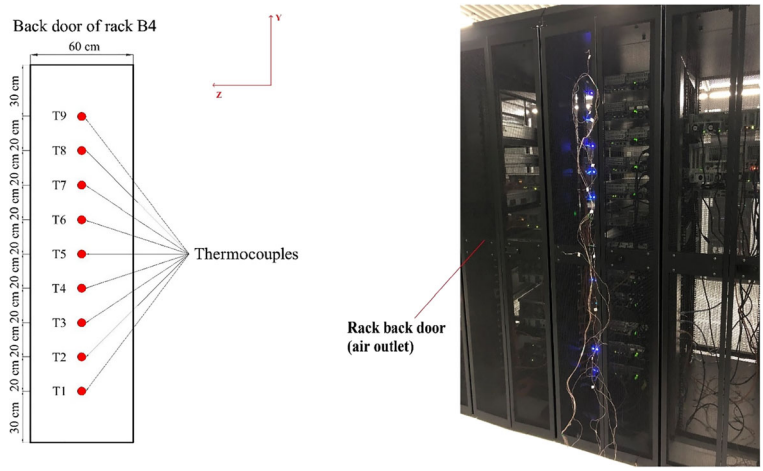

Fig. 4 Arrangement of measuring points in the rack B4

30 cm away from the plenum, and the distance between each adjacent temperature sensor was 20 cm. The exhaust air thermal distribution in the rack B4 was obtained, and the rack hotspot was located. The supply air velocity (SAV) of the rack B4 through the plenum was measured by a handheld airflow anemometer (KIMO VT200/FC300). Ranges and uncertainties of the measuring equipment were shown in Table 2. In the experiment, the data acquisition logger recorded the air temperature measured by the temperature sensor every 10 s, and finally, all the temperature data were transmitted by the data acquisition logger to the personal computer. Each measurement included an adaptive time of 0.5 h and an actual test time of 2 h, i.e. a total of 2.5 h. The adaptive time consists of three parts as follows: the time to change the baffles, time to adjust the angle of baffles, and time which the DC environment recovers to a steady state. Each sensor recorded approximately 1080 temperature values per experiment. To avoid interference from transient temperature fluctuations, the temperature of each measurement point was taken as the arithmetic mean of the measured 1080 temperature values. The reading of the anemometer was between 24 °C and 24.2 °C. Thus, the SAT of the rack B4 was assumed as 24 °C. Meanwhile, the SAV of the rack B4 was measured to be 5.33 m/s.

Table 2 Ranges and uncertainties of the measuring equipment

Measured equipment	Temperature sensor	Handheld airflow anemometer
Range	− 20 °C—400 °C	0.15–30 m/s
Uncertainty	± 0.4%	± 2%

Model setup

The computational fluid dynamics (CFD) modelling study was performed based on the validated model of the same experimental DC. The model was constructed by a commercial CFD software, Fluent Airpak3.0, as shown in Fig. 5. Taking into account such factors as DC scale, racks, servers, and airflow conditions, Abanto et al. (Abanto et al. 2004) considered that the turbulent mixing mode should be chosen as the flow state of the airflow model for the room-level DC. The standard k–ε turbulence model was utilized in the process of numerical simulation due to its satisfactory performance for DC modelling studies (Yuan et al. 2018; Song 2016; Priyadumkol and Kittichaikarn 2014; Almoli et al. 2012). In the calculation of CFD model, the finite volume method was used to transform the differential equation into a discrete equation (Song 2016). This simulation study adopts a steady-state approach, so the phenomena associated with transient flow instability in the DC are not considered, and previous numerical studies (Abanto et al. 2004; Zametaev et al. 2019; Sheth and Saha 2019; Liu et al. 2014; Najjar et al.

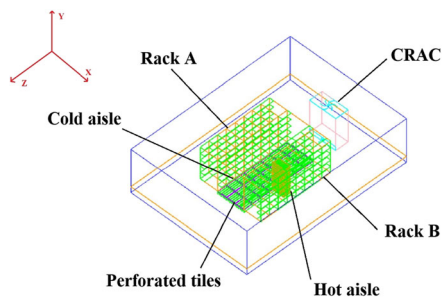

Fig. 5 CFD model of the studied DC

1995) have shown the feasibility and benefits of such an approach. Several assumptions were set for the model as follows: (1) the effects of air leakage and radiation were not considered, (2) air was considered as an incompressible fluid, and (3) the heat dissipation caused by fluid viscosity was ignored.

In actual operation, the server is not always fully loaded. However, running at the full or partial load will have no significant effect on this experiment. Therefore, in the simulation, it was assumed that the server is running at full capacity. In addition, the setting of parameters in the simulation will inevitably deviate from the actual situation, resulting in certain differences between the simulation results and experimental results.

The governing equations for an impressible fluid are expressed as Eqs. (1)–(3), which represents the continuity, momentum, and energy conservation equations, respectively.

$$\nabla \cdot \vec{u} = 0 \tag{1}$$

$$\frac{\partial}{\partial t}\left(\vec{u}\right) + \vec{u} \cdot \nabla \vec{u} = -\nabla p + \nabla \cdot \left(\overline{\overline{T}}\right) + \vec{g} \tag{2}$$

$$\rho c_p \left[\frac{\partial T}{\partial t} + \left(\vec{u} \cdot \nabla\right) T\right] = \nabla \cdot \left(k_{eff} \nabla T\right) + S \tag{3}$$

where $\vec{u}$ represents the average velocity vector, p represents the static pressure, T represents the static temperature, $\vec{g}$ represents the gravitational acceleration vector, V_{eff} and k_{eff} are, respectively, the effective fluid viscosity and thermal conductivity, ρ is the density, S denotes the volumetric heat source, and c_p is the specific heat capacity.

According to Silva-Llanca et al. (Silva-Llanca et al. 2018), the mesh generation is important for the simulation period and simulation accuracy and the success or failure of the simulation depends directly on it. Thus, the following criterion was formulated for the mesh generation as follows: smooth element changes and changes in density in the entire solution domain should be based on the variables (Ni et al. 2017). The calculation reached convergence when the residuals of the velocity in the X, Y, and Z directions reached 10^{-3}, and that for energy was 10^{-6} (Ni et al. 2017; Alkharabsheh et al. 2015). The boundary conditions for this model are given in Table 3. Only racks B3, B4, and B5 are modelled with actual heat power to simplify the numerical model and reduce the simulation time.

The grid number can not only affect the simulation period but also determine the accuracy of the simulation (Ni et al. 2017). A suitable number of meshes can reduce the numerical errors caused by a coarse grid or rounding-off errors caused by dramatic increases in the number of meshes. The grid independence test is widely used in CFD numerical investigations to ensure the feasibility of simulation calculations. Four grid independence tests were performed in this study for four scenarios as follows: with no baffles, with rack baffles, with server terminal baffles, and with the combined baffles. The number of grids was different. The optimum mesh numbers for the scenarios are shown in Fig. 6, in which the hexa-unstructured mesh for this model achieved the balance between good accuracy and high efficiency of the numerical calculation. The mesh quality had been checked automatically by the Grid Quality Inspection Tool of the CFD Airpak3.0 software, and more than 95% of the meshes had a quality of 1 for the four scenarios. The results showed no significant difference when the number of nodes increased, and the minimum gap and maximum side length of all grids were, respectively, 0.001 m and 0.1 m.

Experimental results and mechanism analysis

The validation experiments considered three scenarios (scenarios E0–E2) as presented in Table 4. In scenario

Table 3 Boundary conditions of the CFD model

Item	Description
Walls	Adiabatic
Floor	Adiabatic
Ceiling	Adiabatic
Plenum	Adiabatic
Top of cold aisle containment	Adiabatic
Perforated tiles	45% free air ratio
The front door of racks	65% free air ratio
The rear door of racks	65% free air ratio
CRAC	Inlet fan (supply air temperature 24 °C; supply air velocity 5.33 m/s)
	Outlet fan
Servers	Uniform layout

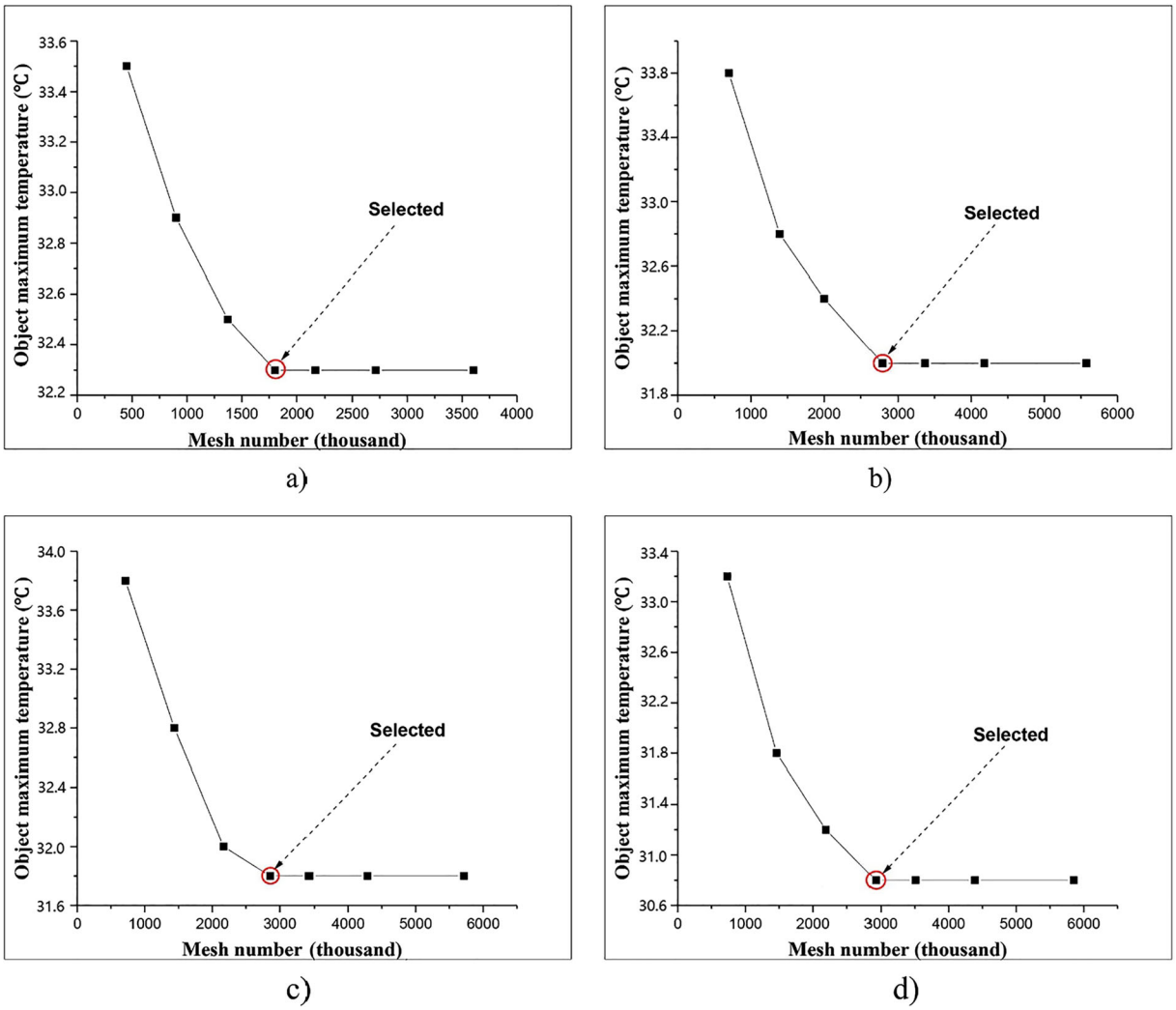

Fig. 6 Object maximum temperature variation with grid number in (**a**) no baffles, (**b**) rack baffles, (**c**) server terminal baffles, and (**d**) combined baffles

E0, there are no baffles introduced. In scenario E1, the angle between the baffle and the vertical downward direction of the rack door is defined as the baffle angle. In scenario E2, the baffle angle is the angle between the baffle and underside of the server. The baffle sizes and angles are selected for the validation from the earlier studies (Qian et al. 2013, 2015). Figure 7 shows the actual mounting positions of the rack baffles and server terminal baffles. Figure 7 (right panel) shows that all servers are equipped with server terminal baffles of the same size and angle except for the lowest server. No baffles were applied in the lowest server because the

Table 4 Three working scenarios in validation experiments

Scenario	E0	E1	E2
Baffle type	NA*	Rack baffles	Server terminal baffles
Baffle size (cm × cm)	NA	20 × 60	46 × 8
Angle (°)	NA	75	45

**NA* not applicable

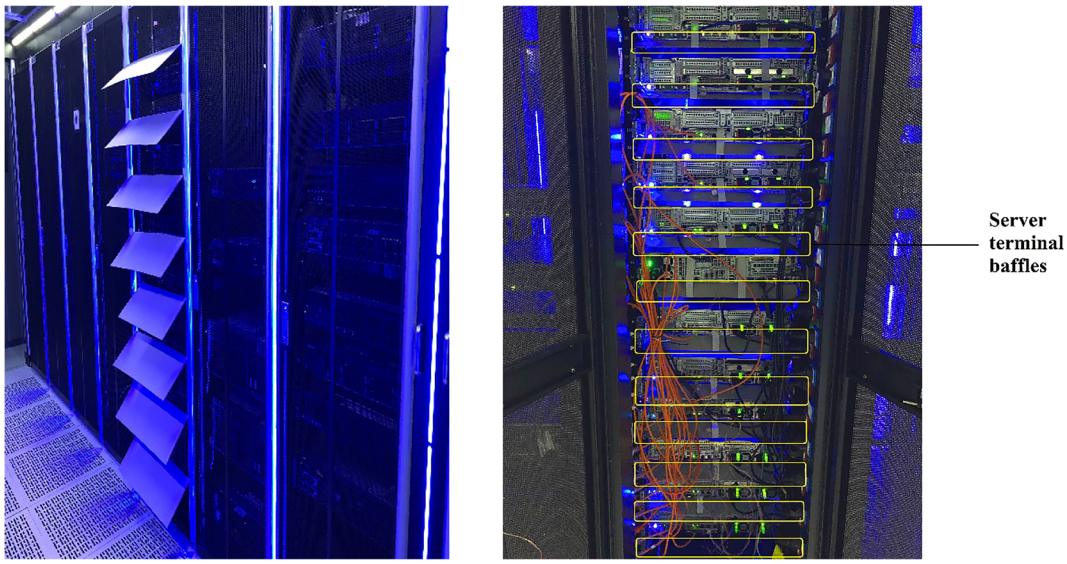

Fig. 7 Installation of rack baffles (left) and server terminal baffles (right)

flow of cold air in the lower channel will be blocked by the baffle.

Reference case without baffles

The experiment was carried out for approximately 2 weeks to obtain the outlet airflow distribution in the rack B4 and examine the influence of different types of baffles on the heat distribution in the rack. Then, the experimental raw data were processed and analysed. In this paper, the average temperature of the nine measurement points was used to describe the overall temperature of the rack B4, and this temperature was used as one of the indicators for determining whether the DC airflow distribution was optimized.

Figure 8 shows the exhaust air temperature of the nine measuring points of the rack B4 with the reference scenario E0 without FBs. The average exhaust temperature of the rack B4 is 28.5 °C. Based on Fig. 8, the temperature of the measuring point at 110 cm distance from the plenum is the highest; therefore, this point is considered as the rack hotspot of the rack B and the temperature of the rack hotspot is 29.1 °C. The maximum temperature difference between the supply temperature and exhaust temperature of the rack reaches 5.1 °C. Furthermore, it can be observed from Fig. 8 that the maximum temperature difference among the nine measurement points reaches 1.9 °C, which indicates that the exhaust temperature of the rack B4 is not uniform enough and there is local overheating.

In the succeeding validation work, the experiments involving scenarios E1–E2 were carried out, and the optimization schemes for the two different baffle systems (rack baffles and server terminal baffles) were respectively set in the rack B4 to investigate their effects on airflow optimization and energy conservation.

Rack baffle system

Figure 9 shows a comparison of the exhaust air temperature for the nine measuring points of the rack B4 in scenarios E0 and E1. In case E0, the temperature of the rack hotspot is approximately 29.1 °C. By applying the optimal rack baffles, the temperature of the rack hotspot

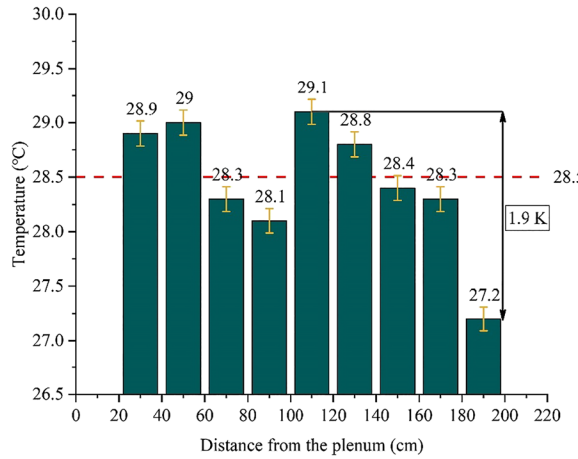

Fig. 8 The exhaust air temperature of nine measuring points of the rack B4 without FBs

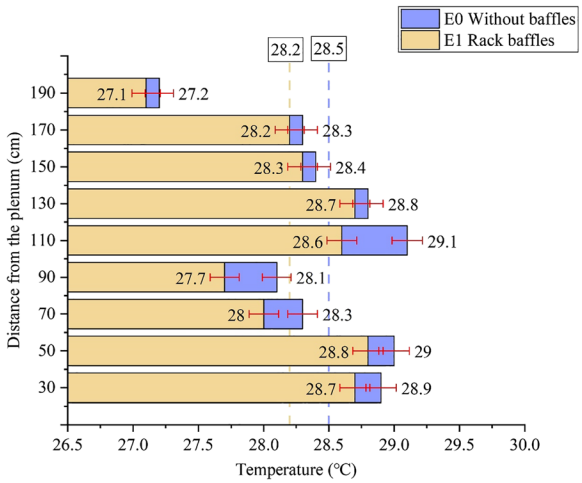

Fig. 9 The exhaust air temperature of nine measuring points of the rack B4 in E0 and E1

drops to 28.8 °C, which is 0.3 °C lower than that without baffles. In addition, the overall temperature is reduced from 28.5 °C to 28.2 °C; thus, the heat accumulation phenomenon of the rack B4 is alleviated.

Figure 10 compares the airflow in the rack B4 with no baffles and with optimal rack baffles. In the case of no baffles, the cold air enters the rack obliquely upwards, and the angle of inclination is large so that the cold air entering the upper part of the rack is more than that below, and the airflow at different heights of the rack is uneven. Therefore, the cold air is tilted up into the rack, causing the bottom of the rack to be insufficiently cooled, resulting in heat accumulation. However, when the optimal rack baffles (20 cm × 75°) are applied, the direction of cold air entering the rack changes from upward tilt to horizontal. With this condition, the airflow at different heights of the rack is more evenly distributed, and the amount of cold air entering the lower part of the rack is guaranteed. Therefore, the optimization mechanism of the rack baffles is changing the direction of the cold air entering the rack, so that the cold air entering different heights of the rack is relatively uniform, and the amount of cold air entering the rack is increased to some extent.

Server terminal baffle system

The exhaust air temperatures of the nine measuring points of the rack B4 in scenarios E0 and E2 are compared in Fig. 11. The overall temperature is reduced from 28.5 °C to 28.1 °C. In the case of no baffles, the temperature of the rack hotspot is approximately 29.1 °C. The temperature of the rack hotspot is reduced by 0.3 °C relative to the case without baffles by applying the optimal server terminal baffles.

Figure 12 shows a comparison of the airflow in the rack B4 with no baffles and that with optimal server terminal baffles. In the case of no baffles, the cold air enters the rack from the cold aisle containment and mostly flows through the path between the servers, forming a bypass airflow and flowing directly out of the rack rear door. However, by applying the server terminal baffles, the direction of the cold air coming out of the channel between the servers is changed, allowing more cold air to participate in cooling the server terminal. Therefore, the optimization mechanism of the server terminal baffles is changing the direction of the bypass airflow between adjacent servers, thereby taking away more heat at the terminal of the servers and improving the cooling efficiency.

The temperatures of the nine different measuring points in all scenarios are compared in Fig. 13. If the temperature is lower than that of E0, it means that the

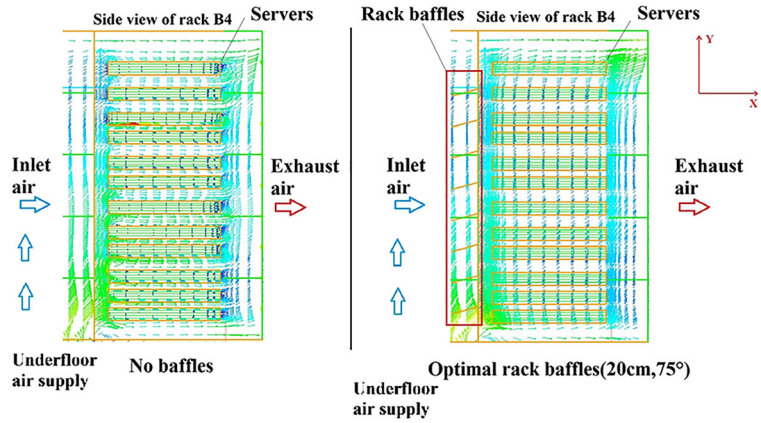

Fig. 10 Airflow in the rack B4 without baffles (left) and with optimal rack baffles (right)

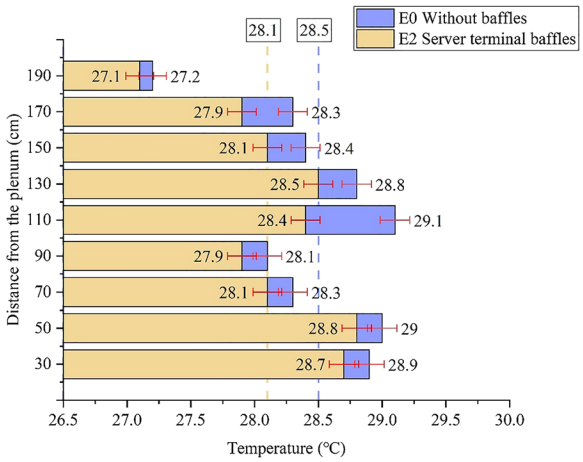

Fig. 11 The exhaust air temperature of nine measuring points of the rack B4 in E0 and E2

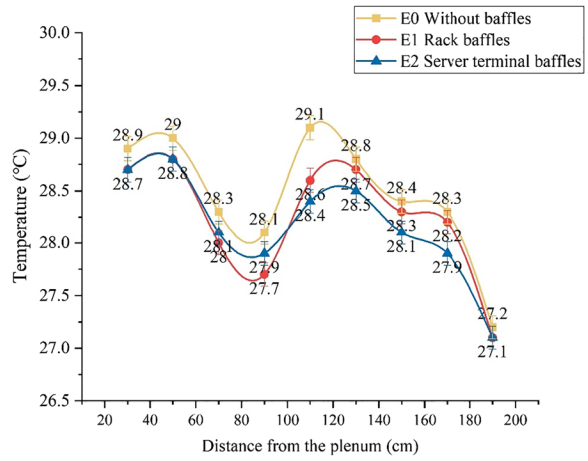

Fig. 13 Variation of overall exhaust air temperature of the rack B4 in E0–E2

thermal performance is better than the reference case. As shown in Fig. 13, the changing trend of the overall temperature for the rack B4 is consistent in E0–E2. The temperature at the measuring point 110 cm from the plenum is the highest, and the temperature at the measuring point 190 cm from the plenum is the lowest. The average temperature is 28.5 °C in scenario E0, and in scenarios E1 and E2, where rack baffles and server terminal baffles are respectively installed, the average temperatures are reduced to 28.2 °C and 28.1 °C, respectively. In addition, the temperature drops of each measuring point are given in Table 5. There are significant temperature drops in scenarios E1 and E2, and the maximum temperature drops of rack hotspot are 0.5 °C and 0.7 °C, respectively.

Considering the overall exhaust temperature, the temperature drops of the rack hotspot and the temperature of the nine measuring points, the rack baffles and server terminal baffles are both able to optimize the airflow distribution and significantly reduce the risk of local hotspot damages to the servers.

The reliability of the model was verified by optimization experiments of the rack baffles and server terminal baffles, and both systems can improve the thermal environment of the DC to a certain extent. According to the optimization mechanism research, the application of rack baffles increases the amount of cold air entering the rack and makes the distribution of cold air entering the cabinet more uniform. In contrast, the application of server terminal baffles improves the utilization of bypass airflow in the channels between adjacent servers, taking away more heat at the terminal of servers. The above researches have shown that the optimization mechanisms of the two systems are different and independent of each other. Through the analysis of the airflow velocity of these two baffle systems, a guess is

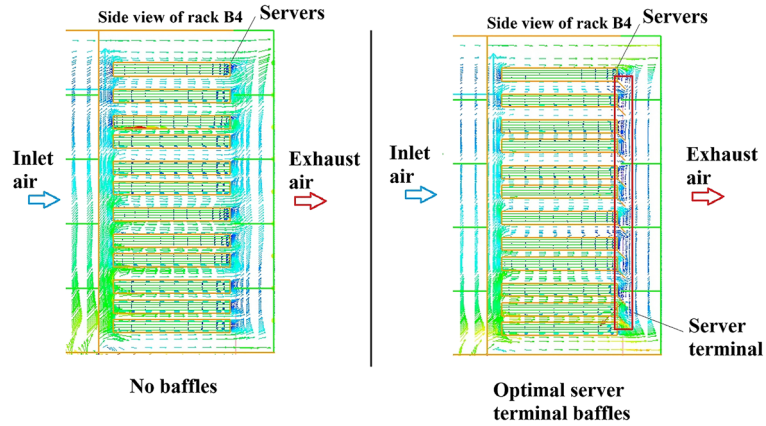

Fig. 12 Airflow without baffles (left) and with optimal server terminal baffles (right)

Table 5 Temperature drop (°C) at each measuring point

Measuring point/cm	30	50	70	90	110	130	150	170	190
E1	0.2	0.2	0.3	0.4	0.5	0.1	0.1	0.1	0.1
E2	0.2	0.2	0.2	0.2	0.7	0.3	0.3	0.4	0.1

proposed that their optimization mechanisms are different and will not affect each other. Thus, the two baffle systems can be easily combined to further optimize the heat distribution and airflow configuration in DCs.

Verification

To validate the accuracy of the simulation results, an experiment of the optimal baffle system combination was carried out. The experimental temperature values in the nine measurement points of the rack B4 in two different situations (without baffles vs. with the optimal combination system) are compared in Fig. 14. The temperature trends in both cases are basically consistent. In the case of installing the optimal baffle combination system, the temperature of each measurement point is slightly lower than the original condition in the experimental data, and the largest temperature drop is 0.9 °C. The combined baffle system can effectively reduce the temperature of the hotspot and make the heat distribution in the DC more uniform.

Overall, the exhaust air temperature distribution and thermal environment were optimized when the combined baffle system was applied. The application could realize the following optimization as follows: (i) the temperatures of the test points were all below 29 °C, (ii) the maximum temperature drop achieved was approximately 0.9 °C, (iii) the temperature of the hotspot in the rack B4 reduced by 0.7 °C from 29.1 °C to 28.4 °C, and (iv) the heat accumulation was eliminated and the thermal environment was improved.

Figure 15 illustrates the deviation of the nine measuring points between the experimental and numerical results. As shown in the figure, the maximum deviations are all below 10%. This proves that the simulations are very close to the experimental values. The deviation between the experimental data and numerical results of each measurement point is listed in Table 6. It can be observed that the numerical results agree well with the experimental results.

Combined rack and server baffle system

To further demonstrate the independence of these two baffle systems, 11 sets of simulations were performed, namely, scenario 1 (5 cases with 20 cm × 75° rack

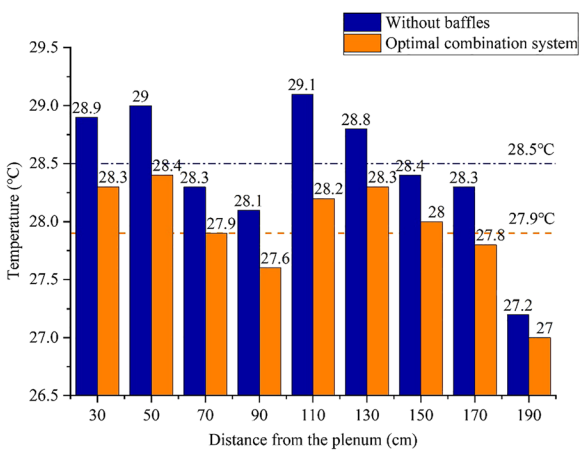

Fig. 14 Comparison of experimental values under two different conditions

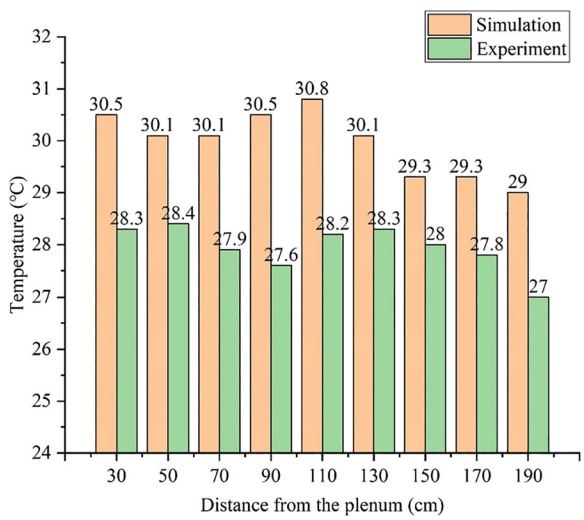

Fig. 15 The deviation between measured and simulated results of nine measuring points in the rack B4

Table 6 Deviation of each measuring point

Measuring point	1	2	3	4	5	6	7	8	9
Deviation (°C)	0.2	0.2	0.2	0.2	0.7	0.3	0.3	0.4	0.1

baffles and 8 cm × 46 cm SLTBs with five baffle angles of 15°, 30°, 45°, 60°, and 75°) and scenario 2 (6 cases with 8 cm × 45° SLTBs and 20 cm × 60 cm rack baffles with six baffle angles of 15°, 30°, 45°, 60°, 75°, and 90°). The optimal size and angle of the combined baffle system were obtained. In addition, the optimal airflow configuration and heat distribution characteristics were analysed. Figure 16 showed a sketch of the baffles' installation of the combined system. Rack baffles are installed at the entrance of the front door of the rack B4 to change the direction of the cold air entering the servers, so that the cold air entering the rack at different heights is relatively uniform, and the amount of cold air entering is increased. The SLTBs is installed at the server end to change the direction of the bypass airflow at the outlet, thereby taking away more heat from the server terminal and improving the cooling efficiency.

Simulation analysis of the combined system

The numerical simulation analysis considered three scenarios (scenarios S0–S2) and 12 cases, as listed in Table 7. The heat distribution characteristics of the DC in each combination case were analysed, including the possibility that the optimal scheme of different baffle systems can be simply superimposed.

Simulation results of combined baffle systems

Based on the optimal rack baffle (20 cm × 75°), different angles of server terminal baffles were installed at the server to further optimize the thermal environment. Figure 17 shows the exhaust air temperature profiles (the plane of the back door) of the rack B4 in the scenarios S0 and S1. In these scenarios, there is all significant heat

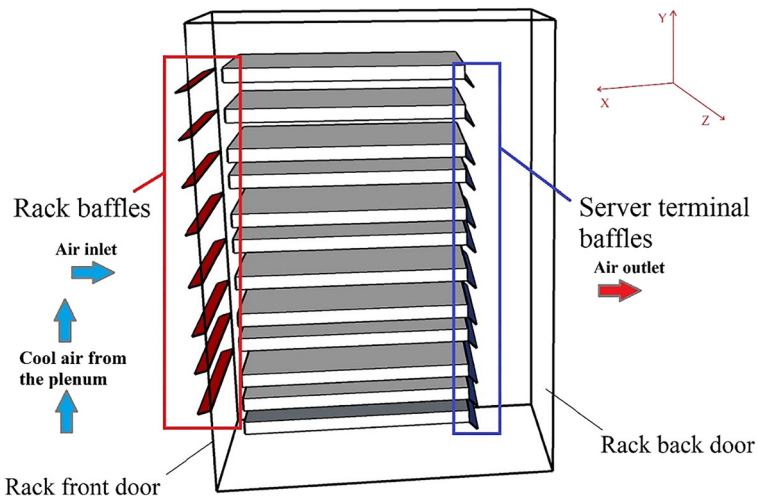

Fig. 16 A sketch of the baffles' installation of the combined system

Table 7 The analysed scenarios of the combined baffle system

Simulation S	S0	S1	S2
Rack baffle size (cm × cm)	NA*	20 × 60	20 × 60
Rack baffle angle (°)	NA	75	15/30/45/60/75/90
Server terminal baffle size (cm × cm)	NA	46 × 8	46 × 8
Server terminal baffle angle (°)	NA	15/30/45/60/75	45

*NA not applicable

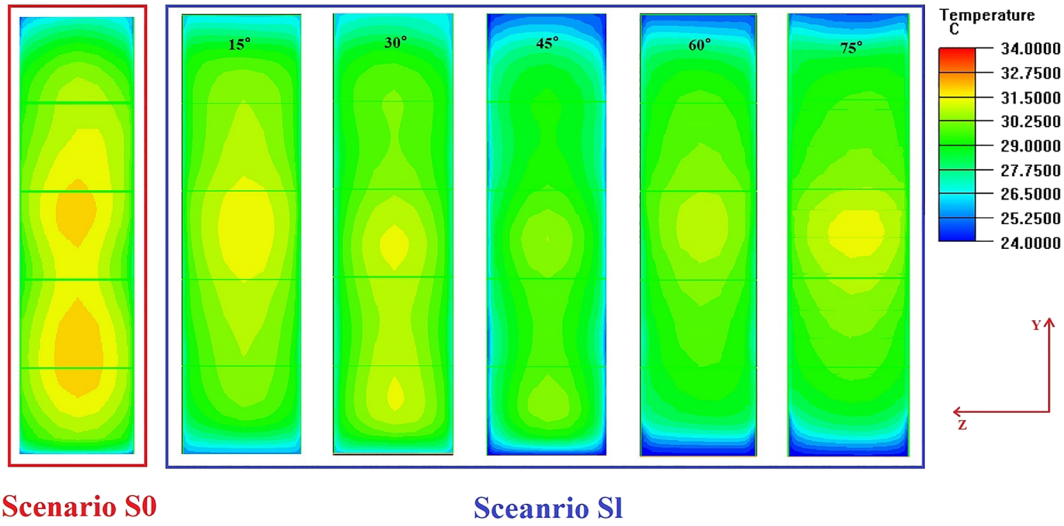

Fig. 17 Exhaust air temperature distribution in the rack B4 for scenarios S0 and S1

accumulation in the middle portions of the rack B4. When the 15° server terminal baffles are used, the heat accumulation in the lower part of the rack B4 does not improve, but instead deteriorates and becomes central heat accumulation. When the angle of server terminal baffles is 30°, the heat accumulation is relieved to some extent. When the baffle angles are 45°, 60°, and 75°, the heat accumulation range of the rack B4 is slightly reduced, the hotspot temperature of the rack is lowered, the heat accumulation of the rack B4 is greatly improved, and the thermal environment is improved. In these three cases, the overall temperature of the rack B4 has dropped. Although the temperature of the rack hotspot decreases when the baffle angles are 60° and 75°, the heat accumulation problem and thermal environment are not improved. Both the heat accumulation problem and thermal environment are improved when the baffle angle is 45°. The exhaust air temperature distribution in the upper and lower parts of the rack B4 is relatively uniform in this case. Therefore, when the rack baffles are fixed and the angle of the server terminal baffles is 45°, the combined system performs best in eliminating heat accumulation and improving the thermal environment.

Figure 18 depicts the exhaust air temperatures of the rack B4 in S0 and S1. Compared with those in scenario S0, the temperatures of the recording points in S1 have different degrees of declines. In particular, when the angle of the server terminal baffles is 45°, the temperatures of all recording points are below 31 °C and the temperature drop at measuring point NO.7 is the largest. In addition, the maximum temperature difference between the nine recording points in S1 is 1.8 °C, and the temperature distribution is relatively uniform. Therefore, it can be observed from the temperature changes of the nine points that the heat distribution performance of the air outlet of the rack B4 is optimal when the angle of the server terminal baffles in S1 is 45°. Table 8 shows the standard deviation of the temperatures recorded by rack B4 in S0 and S1. When the angle of the server terminal baffles in S1 is 45°, the standard deviation of the minimum of 1.18, thus the temperature of rack B4 is more stable than that in other cases.

Similarly, based on the optimal server terminal baffles (8 cm × 45°), baffles with different angles were

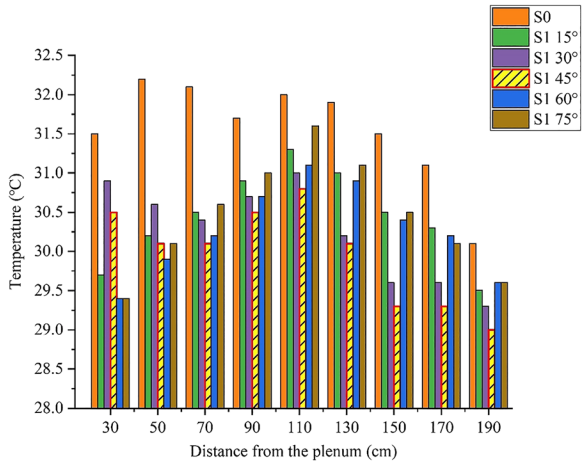

Fig. 18 Exhaust air temperatures of nine temperature recording points for the rack B4 in S0 and S1

Table 8 The standard deviation of the exhaust temperature at rack B4 in S0 and S1

Case	S0	S1_15°	S1_30°	S1_45°	S1_60°	S1_75°
Standard deviation	1.37	1.32	1.27	1.18	1.24	1.30

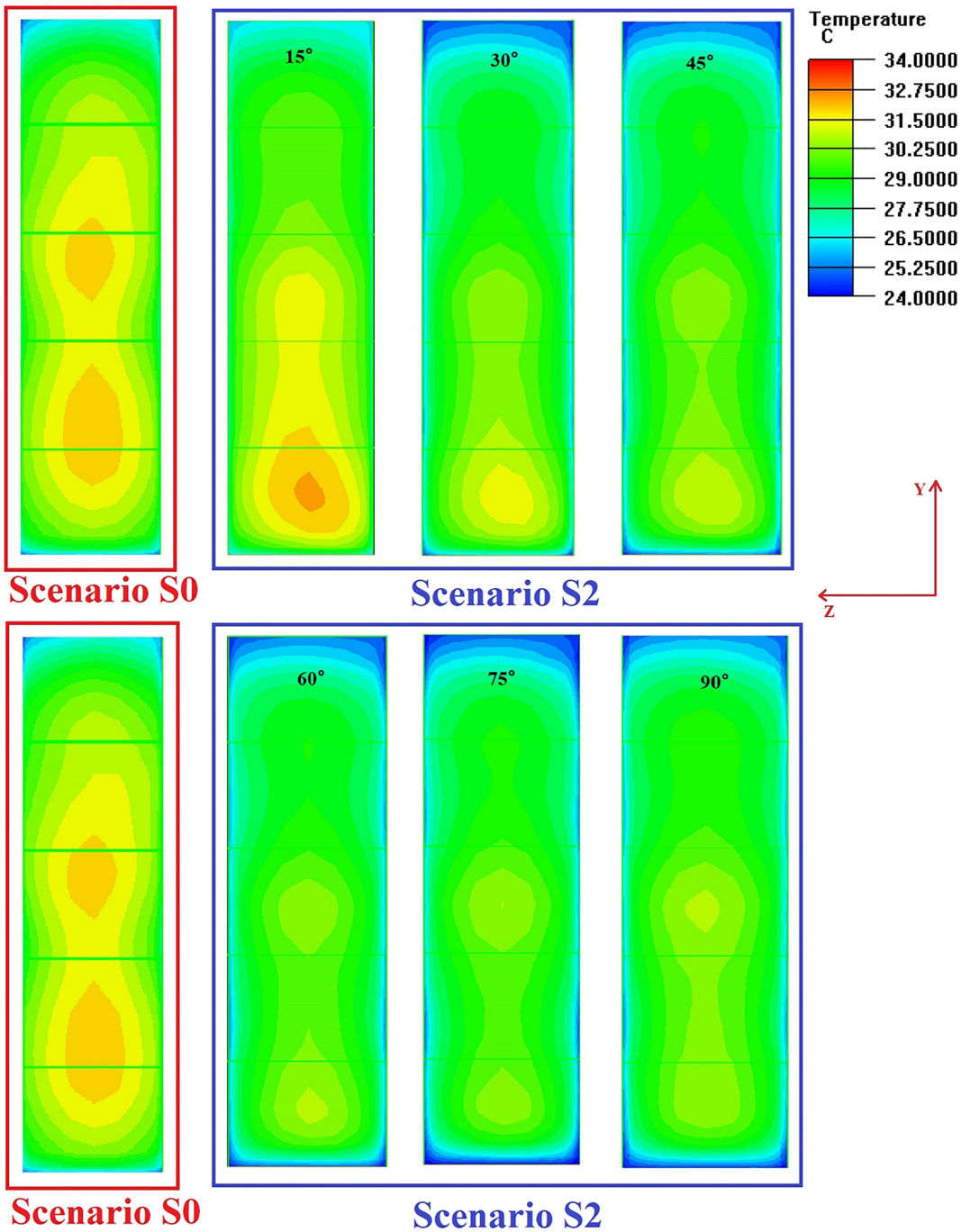

Fig. 19 Exhaust air temperature distribution in the rack B4 for scenarios S0 and S2

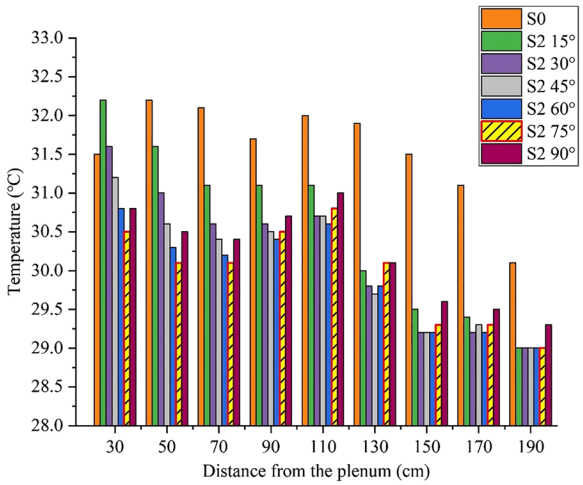

Fig. 20 Exhaust air temperatures of nine temperature recording points of the rack B4 in S0 and S2

installed on the front door of the rack to further optimize the thermal environment. Figure 19 shows the exhaust temperature profile (the plane of the back door) of the rack B4 in scenarios S0 and S2. In scenario S0, there is significant heat accumulation in the lower and middle portions of the rack B4. When the server terminal baffles and rack baffles are used at the same time, the heat accumulation in the middle and lower portions of the rack B4 is lower. As the angle increases, the heat accumulation improvement is more evident, and the temperature of the rack hotspot is reduced. However, when the angle is increased to 90°, the temperature of the rack hotspot rises again. The exhaust air temperature distribution in the upper and lower parts of the rack B4 is relatively uniform when the angle of the rack baffles is 75°. Therefore, when the server terminal baffles are fixed and the angle of the rack baffles is 75°, the hotspot temperature of the rack is the lowest, and the heat distribution in the rack is the most uniform.

Figure 20 shows the exhaust temperature of the rack B4 in S0 and S2. Compared with those in scenario S0, the temperatures of the recording points in S2 have different degrees of declines. Especially when the angle of the rack baffles is 75°, the temperature of the recording point is lower than 31 °C, and the temperature at the measuring point NO.7 is the most optimized. In addition, the temperature distribution is relatively uniform. Therefore, considering the temperature change of the nine temperature recording points of the rack B4, when the angle of the rack baffles in S2 is 75°, the heat distribution performance of the rack B4 is optimal. Table 9 shows the standard deviation of the temperature recorded by frame B4 in S0 and S2. When the angle of the server terminal baffles in S2 is 75°, the standard deviation of the minimum of 1.22, thus the temperature of rack B4 is more stable than that in other cases.

The simulation validation shows that when the rack baffles are fixed at 20 cm × 75°, the angle of the server terminal baffles is changed, and the optimal heat distribution in the rack B4 is obtained at 8 cm × 45°. Conversely, when the server terminal baffles are fixed at 8 cm × 45°, the thermal environment of the rack is optimal when the rack baffles are 20 cm × 75°. The simulation results of the above two scenarios show that considering the rack hotspot temperature and heat distribution uniformity of the rack B4, the combined baffle system of 20 cm × 75° rack baffle and 8 cm × 45° server terminal baffles has the best performance in eliminating heat accumulation and improving heat distribution. In addition, the above analysis proves that the optimization mechanisms of the two methods are different and are not affected by each other. Therefore, the two baffle systems can be easily combined to further optimize the heat distribution and airflow configuration in DCs.

Optimal combination of baffle system

Figure 21 shows a comparison of the temperature profiles of the exhaust air temperature in four different situations (no baffles, only optimal rack baffles, optimal server terminal baffles, optimal combined baffles). When the optimal rack baffles (20 cm × 75°) are installed together with the optimal server terminal baffles, the temperature of the rack hotspot is significantly reduced and the temperature distribution in the rack is more uniform. Figure 22 shows the airflow without baffles and that with the optimum combined baffles. A more uniform air supply is achieved by applying the combined baffle system. With this condition, the

Table 9 The standard deviation of the exhaust temperature at rack B4 in S0 and S2

Case	S0	S2_15°	S2_30°	S2_45°	S2_60°	S2_75°	S2_90°
Standard deviation	1.37	1.41	1.33	1.26	1.22	1.22	1.25

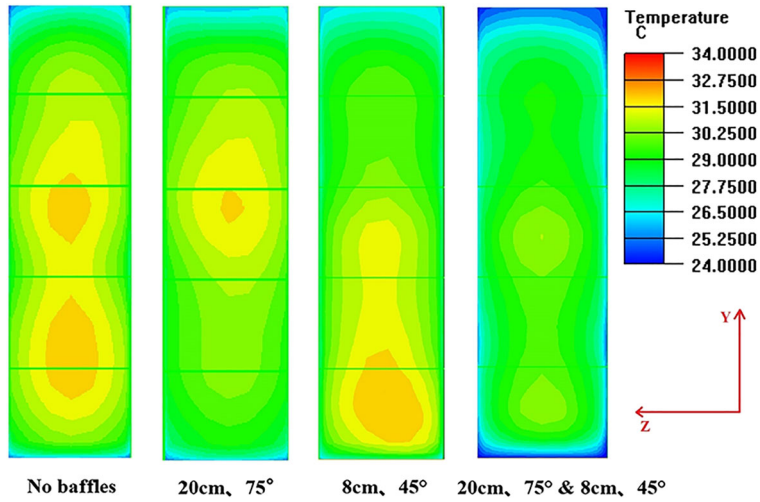

Fig. 21 Comparison of exhaust air temperature cloud maps under different conditions

temperature of the rack hotspot is reduced relative to the original state and the heat distribution in the rack B4 is the most uniform. Both the heat accumulation problem and thermal environment are improved when the combination of baffle systems is applied.

The 12 sets of simulations show that the applications of the two systems are not affected by each other; thus, the two baffle systems can be simply combined to further optimize the heat distribution in the DC airflow configuration and the air outlet of racks. With this strategy, the temperature of each measuring point of the rack is lower than 29 °C, and the temperature of the rack hotspot is reduced by 0.7 °C.

Conclusions

A new method of combining rack and server baffle systems was proposed innovatively in this study, which can be applied to high-density DCs with uniform servers without changing the overall structure of DCS. It is suitable for both new and renovated DCs and the optimization effects of the rack baffles and server terminal baffles on the thermal distribution in the DC were validated by experiments. In addition, the optimization mechanisms of the different baffle systems and the effect on the performance of the best baffle combinations were investigated. The optimal combined simulation model was validated by field experiments. The experimental results were in good agreement with the numerical results and the main conclusions are as follows:

(1) Based on the velocity field analysis and numerical simulation, the optimization mechanisms of the two baffle systems are different and do not affect each other; therefore, they can be easily combined to further optimize the heat distribution in the DC.

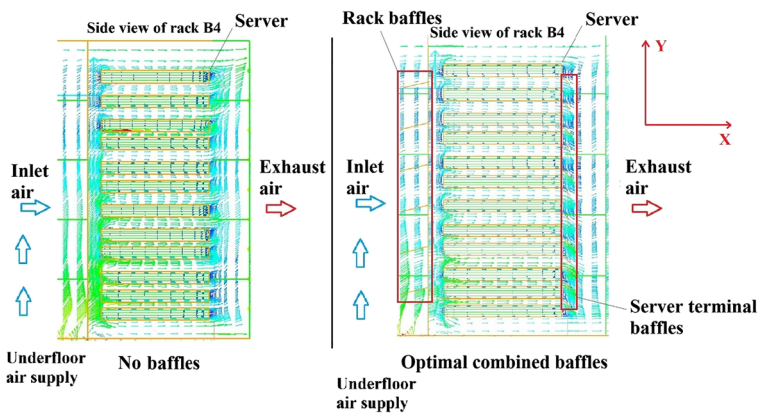

Fig. 22 Airflow without baffles (left) and with optimum combined baffles (right)

(2) The combined system of the optimal server terminal baffles (8 cm × 45°) and optimal rack baffles (20 cm × 75°) achieved the most uniform heat distribution, which greatly reduces the risk of local hotspot damages to the servers.
(3) The exhaust air uniformity in all server racks was significantly improved by applying the rack baffles and server terminal baffles. Both the rack baffles and server terminal baffles can reduce the rack hotspots by 0.3 °C, while the combined baffles system can reduce the rack hotspots by 0.7 °C

Acknowledgments We acknowledge the assistance provided by the Information Centre of Nanjing Tech University in conducting the onsite experiments.

Compliance with ethical standards

Conflict of interest The authors declare that they have no conflict of interest.

References

Abanto, J., Barrero, D., Reggio, M., & Ozell, B. (2004). Airflow modelling in a computer room. *Building and Environment., 39*(12), 1393–1402.

Alkharabsheh, S., Fernandes, J., Gebrehiwot, B., Agonafer, D., Ghose, K., Ortega, A., et al. (2015). A brief overview of recent developments in thermal management in data centers. *Journal of Electronic Packaging Transactions of the Asme, 137*(4):040801.1–040801.19.

Almoli, A., Thompson, A., Kapur, N., Summers, J., Thompson, H., & Hannah, G. (2012). Computational fluid dynamic investigation of liquid rack cooling in data centres. *Applied Energy., 89*(1), 150–155.

Ashrae, T. 9.9 (2011) Thermal guidelines for data processing environments–expanded data center classes and usage guidance. Whitepaper prepared by ASHRAE technical committee (TC). 2011;9.

Avgerinou, M., Bertoldi, P., & Castellazzi, L. (2017). Trends in data centre energy consumption under the European code of conduct for data centre energy efficiency. *Energies., 10*, 1470.

Boucher, T. D., Auslander, D. M., Bash, C. E., Federspiel, C. C., editors. (2006) Viability of dynamic cooling control in a data center environment. Thermal and Thermomechanical Phenomena in Electronic Systems, 2004 ITHERM '04 The Ninth Intersociety Conference on.

Chauhan, A., & Kandlikar, S. G. (2019). Characterization of a dual taper thermosiphon loop for CPU cooling in data centers. *Applied Thermal Engineering., 146*, 450–458.

Cho, J., & Kim, Y. (2016). Improving energy efficiency of dedicated cooling system and its contribution towards meeting an energy-optimized data center. *Applied Energy., 165*, 967–982.

Daraghmeh, H. M., & Wang, C.-C. (2017). A review of current status of free cooling in datacenters. *Applied Thermal Engineering., 114*, 1224–1239.

Dayarathna, M., Wen, Y., & Fan, R. (2016). Data center energy consumption modeling: a survey. *IEEE Communications Surveys & Tutorials., 18*(1), 732–794.

Dewan, A., & Srivastava, P. (2015). A review of heat transfer enhancement through flow disruption in a microchannel. *Journal of Thermal Science., 24*(3), 203–214.

Habibi Khalaj, A., & Halgamuge, S. K. (2017). A review on efficient thermal management of air- and liquid-cooled data centers: from chip to the cooling system. *Applied Energy., 205*, 1165–1188.

Ham, S.-W., Kim, M.-H., Choi, B.-N., & Jeong, J.-W. (2015a). Energy saving potential of various air-side economizers in a modular data center. *Applied Energy., 138*, 258–275.

Ham, S.-W., Park, J.-S., & Jeong, J.-W. (2015b). Optimum supply air temperature ranges of various air-side economizers in a modular data center. *Applied Thermal Engineering., 77*, 163–179.

Joshi, Y., Joshi, Y. (2012). Energy Efficient Thermal Management of Data Centers.

Kurkjian, C., & Glass, J. (2007). Meeting the needs of 24/7 data centers. *ASHRAE Journal., 49*(2), 24.

Le Masson, S., Nörtershäuser, D., Mondieig, D., & Louahlia-Gualous, H. (2012). Towards passive cooling solutions for mobile access network. *Annals of Telecommunications-Annales des Télécommunications, 67*(3–4), 125–132.

Liu, C.-l., Wolfersdorf, J., & Zhai, Y.-n. (2014). Time-resolved heat transfer characteristics for steady turbulent flow with step changing and periodically pulsating flow temperatures. *International Journal of Heat and Mass Transfer., 76*, 184–198.

Ma, Y., Ma, G., Zhang, S., & Zhou, F. (2016). Cooling performance of a pump-driven two phase cooling system for free cooling in data centers. *Applied Thermal Engineering., 95*, 143–149.

Mittal, S. (2014). Power management techniques for data centers: A survey. arXiv preprint arXiv:14046681.

Nada, S. A., & Elfeky, K. E. (2016). Experimental investigations of thermal managements solutions in data centers buildings for different arrangements of cold aisles containments. *Journal of Building Engineering., 5*, 41–49.

Najjar, F. M., Thomas, B. G., & Hershey, D. E. (1995). Numerical study of steady turbulent flow through bifurcated nozzles in continuous casting. *Metallurgical & Materials Transactions B., 26*(4), 749–765.

Ni, J., Jin, B., Zhang, B., & Wang, X. (2017). Simulation of thermal distribution and airflow for efficient energy consumption in a small data centers. *Sustainability., 9*(4), 664.

Oró, E., Depoorter, V., Garcia, A., & Salom, J. (2015). Energy efficiency and renewable energy integration in data centres. Strategies and modelling review. *Renewable and Sustainable Energy Reviews., 42*, 429–445.

Pawlish, M., Aparna, S. V., editors. (2010). Free cooling: a paradigm shift in data centers. 2010 Fifth International

Conference on Information and Automation for Sustainability: IEEE.

Phan, L., Hu, B., & Lin, C.-X. (2019). An evaluation of turbulence and tile models at server rack level for data centers. *Building and Environment., 155*, 421–435.

Priyadumkol, J., & Kittichaikarn, C. (2014). Application of the combined air-conditioning systems for energy conservation in data center. *Energy and Buildings., 68*, 580–586.

Qian, X., Li, Z., & Li, Z. (2013). A thermal environmental analysis method for data centers. *International Journal of Heat and Mass Transfer., 62*, 579–585.

Qian, X., Li, Z., & Li, Z. (2015). Entransy and exergy analyses of airflow organization in data centers. *International Journal of Heat and Mass Transfer., 81*, 252–259.

Sakanova, A., Alimohammadi, S., McEvoy, J., Battaglioli, S., & Persoons, T. (2019). Multi-objective layout optimization of a generic hybrid-cooled data centre blade server. *Applied Thermal Engineering., 156*, 514–523.

Schmidt, R. R., Cruz, E., & Iyengar, M. (2005). Challenges of data center thermal management. *IBM Journal of Research and Development, 49*(4.5), 709–723.

Schmidt, R. R., Iyengar, M., & van der Mersch, P. L. (2007). Best practices for data center thermal and energy management-review of literature/DISCUSSION. *ASHRAE Transactions., 113*, 206.

Sheth, D. V., & Saha, S. K. (2019). Numerical study of thermal management of data centre using porous medium approach. *Journal of Building Engineering., 22*, 200–215.

Silva-Llanca, L., Ortega, A., Fouladi, K., del Valle, M., & Sundaralingam, V. (2018). Determining wasted energy in the airside of a perimeter-cooled data center via direct computation of the exergy destruction. *Applied Energy., 213*, 235–246.

Siriwardana, J. (2012). Energy efficiency enhancement and optimisation for data centres: Ph. D. thesis, The University of Melbourne, Mechanical Engineering Department;

Siriwardana, J., Halgamuge, S. K., Scherer, T., & Schott, W. (2012). Minimizing the thermal impact of computing equipment upgrades in data centers. *Energy and Buildings., 50*, 81–92.

Siriwardana, J., Jayasekara, S., & Halgamuge, S. K. (2013). Potential of air-side economizers for data center cooling: a case study for key Australian cities. *Applied Energy., 104*, 207–219.

Song, Z. (2016). Thermal performance of a contained data center with fan-assisted perforations. *Applied Thermal Engineering., 102*, 1175–1184.

Wang, I. N., Tsui, Y.-Y., & Wang, C.-C. (2015). Improvements of airflow distribution in a container data center. *Energy Procedia, 75*, 1819–1824.

Wang, J., Zhang, Q., Yoon, S., & Yu, Y. (2019a). Reliability and availability analysis of a hybrid cooling system with water-side economizer in data center. *Building and Environment., 148*, 405–416.

Wang, J., Zhang, Q., Yoon, S., & Yu, Y. (2019b). Impact of uncertainties on the supervisory control performance of a hybrid cooling system in data center. *Building and Environment., 148*, 361–371.

Yuan, X., Wang, Y., Liu, J., Xu, X., & Yuan, X. (2018). Experimental and numerical study of airflow distribution optimisation in high-density data centre with flexible baffles. *Building and Environment., 140*, 128–139.

Yuan, X., Zhou, X., Liu, J., & Wang, Y. (2019). Risto k, Xu X. experimental and numerical investigation of an airflow management system in data center with lower-side terminal baffles for servers. *Building and Environment., 155*, 308–319.

Zametaev, V. B., Gorbushin, A. R., & Lipatov, I. I. (2019). Steady secondary flow in a turbulent mixing layer. *International Journal of Heat and Mass Transfer., 132*, 655–661.

Zhang, Q., Cheng, L., & Boutaba, R. (2010). Cloud computing: state-of-the-art and research challenges. *Journal of internet services and applications., 1*(1), 7–18.

Zhang, H., Shao, S., Xu, H., Zou, H., & Tian, C. (2014). Free cooling of data centers: a review. *Renewable and Sustainable Energy Reviews., 35*, 171–182.

Zhang, M., An, Q., Long, Z., Pan, W., Zhang, H., & Cheng, X. (2017). Optimization of airflow Organization for a Small-scale Date Center Based on the cold aisle closure. *Procedia Engineering., 205*, 1893–1900.

Zhang, K., Zhang, Y., Liu, J., & Niu, X. (2018). Recent advancements on thermal management and evaluation for data centers. *Applied Thermal Engineering., 142*, 215–231.

Zou, S., Zhang, Q., Yu, Y., Yue, C., Wang, J., & Ma, X. (2019). Field study on the self-adaptive capacity of multi-split heat pipe system (MSHPS) under non-uniform conditions in data center. *Applied Thermal Engineering, 160*, 113999.